



New trapezoid-shaped Frisch-grid ionization chamber for low-energy particle measurements

Tianli Qiu^{1,2}, Yuansheng Yang^{1,2}, Xiaohua Yuan^{1,2}, Peng Ma^{1,2}, Meng Li^{1,2}, Junwei Zhang³, Dong Guo⁴, Yuxuan Yang^{6,7}, Xianglun Wei^{1,2}, Zhoubo He^{1,2}, Xiaohao Yin^{1,2}, Xinjie Huang^{1,2}, Haichuan Zou⁵, Zhijie Li^{1,2}, Zhixuan He⁵, Chengui Lu^{1,2}, Rongjiang Hu^{1,2}, Hooi Jin Ong^{1,2,9,10}, Herun Yang^{1,2,a}, Zhigang Xiao⁴, Hongwei Wang^{2,6,8}, Limin Duan^{1,2}

¹ Institute of Modern Physics, Chinese Academy of Sciences, Lanzhou 730000, China

² School of Nuclear Science and Technology, University of Chinese Academy of Sciences, Beijing 100049, China

³ North China University of Water Resources and Electric Power, Zhengzhou 450000, China

⁴ Department of Physics, Tsinghua University, Beijing 100084, China

⁵ School of Nuclear Science and Technology, Lanzhou University, Lanzhou 730000, China

⁶ Shanghai Institute of Applied Physics, Chinese Academy of Sciences, Shanghai 201800, China

⁷ School of Physics and Microelectronics, Zhengzhou University, Zhengzhou 450001, China

⁸ Shanghai Advanced Research Institute, Chinese Academy of Sciences, Shanghai 201210, China

⁹ Joint Department for Nuclear Physics, Lanzhou University and Institute of Modern Physics, Chinese Academy of Sciences, Lanzhou 730000, China

¹⁰ Research Center for Nuclear Physics, Osaka University, Ibaraki, Osaka 567-0047, Japan

Received: 29 August 2022 / Accepted: 23 October 2022 / Published online: 31 October 2022
© The Author(s) 2022

Abstract A new trapezoid-shaped Frisch-grid ionization chamber (TFG-IC) has been built as a part of a $\Delta E - E$ telescope system for the detection and identification of charged particles at energies down to a few MeV. To study the effect of the drift electric field uniformity, two types of sealed windows, namely a pair of SSA (split-strip aluminized mylar film) and a pair of DSA (double-sided aluminized mylar film) sealed windows have been investigated. The detector's performances were studied using a standard ^{241}Am source at different gas pressures, and the total energy-deposit resolution achieved is about 1.1%(FWHM). The $\Delta E - E$ telescope, which was composed of TFG-IC and a DSSSD (double-sided silicon strip detector), has been tested using a three-component α source and the ^{241}Am source under laboratory conditions. The results show that the energy resolution with the SSA sealed windows which provide uniform drift electric field has a smaller fluctuation than that with the DSA ones; the fluctuations are about 1% and 4% for the former and the latter, respectively. Simulations using the COMSOL software also confirmed the electric-field distortion at the edge of the detector with the DSA windows. A correlation curve between energy resolution and energy deposit of charged particles at various gas pressures and for two gas species is derived for TFG-IC with the SSA sealed windows using

the measurement with the ^{241}Am source. Incorporating the above results, we performed Monte Carlo simulations to evaluate the particle-identification capability of the telescope. The results show that the telescope can be extended to the identification of low-energy particles.

1 Introduction

Heavy ion collision is one of the most important methods in the laboratory to understand the isospin-dependent equation of state of nuclear matter. The emission time scale of isospin-dependent particles carries information about the isospin properties. Accelerator facilities such as SPIRAL2 at GANIL [1], SPES at LNL [2], FAIR at GSI [3], FRIB at MSU [4], RIBF at RIKEN [5], FRIBS at LNS-Catania [6] and HIRFL at IMP [7], providing high-intensity radioactive beams, will cover a broad range of isospin (N/Z) ratios; here N and Z are the neutron and atomic numbers, respectively. These measurements must be carried out with both good energy and angular resolution in order to investigate multi-particle correlations. However, the intensity of the most exotic beams will always be low, thus necessitating the development of high efficiency arrays capable of isotopic identification.

^a e-mail: yanghr@impcas.ac.cn (corresponding author)

Many laboratories in the world have built telescope arrays based on silicon strip position-sensitive detectors such as MUST2 [8], INDRA [9,10], LASSA [11], NIMROD [12], FARCOS [13,14] and FAZIA [15], gas-detector-based telescopes such as CSHINE [16,17], as well as the light charged-particle detector array at SLEGS [18]. However, these methods lack detection and identification capability of a large number of low-energy particles produced over a wide range of beam energies. Detailed studies of multi-particle correlations will require isotope identification of fragments over a wider range of Z , A , energy and angles than is currently possible, and hence an efficient telescope system with good energy and angular resolution, and capable of isotope identification will need to be developed.

To improve the present experimental capabilities, we have developed a trapezoid-shaped Frisch-grid ionization chamber (TFG-IC) as part of a telescope system to cover the identification of low-energy incident particles. Particular design consideration was given to realize an efficient arrangement of a multiple-telescope detector system with minimum dead area. It is difficult to design a Frisch-grid ionization chamber with an irregular structure because the electric field uniformity in the sensitive region largely determines whether or not the primary electrons can be collected well. A special shielding-window structure is designed to improve the drifting electric field. The feasibility of the scheme was confirmed through measurements with an α source for TFG-IC, and also for a system that incorporates TFG-IC and a silicon detector under laboratory conditions.

2 Construction and operation

2.1 Design constraints

Like several other earlier ionization-chamber based telescopes, we plan to use TFG-IC as an energy-loss (ΔE) detector in nuclear physics experiments to measure energy losses of charged particles emitted from incident ion beams or nuclear reactions [19,20]. The ERDA (elastic recoil detection analysis) system developed at the University of Tokyo was able to identify light ions of elements from Lithium (Li) to Fluorine (F) [21]. In the test results of GASTLY detector, protons and α particles were significantly distinguished [22]. The FG-IC telescope designed by Ma et al. [23] has good particle identification ability for heavy particles ^{16}O and ^{17}F .

We have constructed a TFG-IC-based charged-particle telescope system. The entire detector assembly was housed in separable aluminum boxes, which were designed to provide mechanical support, relative alignment, and electromagnetic shielding of the detectors, as shown in Fig. 1. TFG-IC was selected to be the first layer of the telescope to enable detection of low-velocity highly-ionizing particles. A 300-

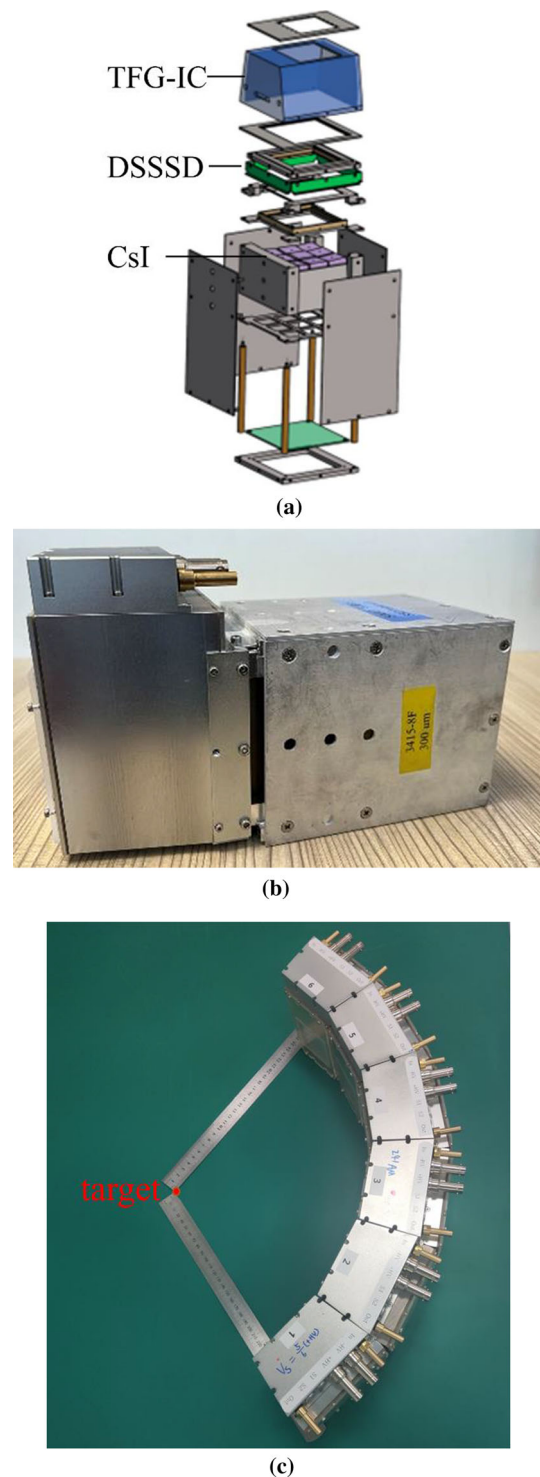
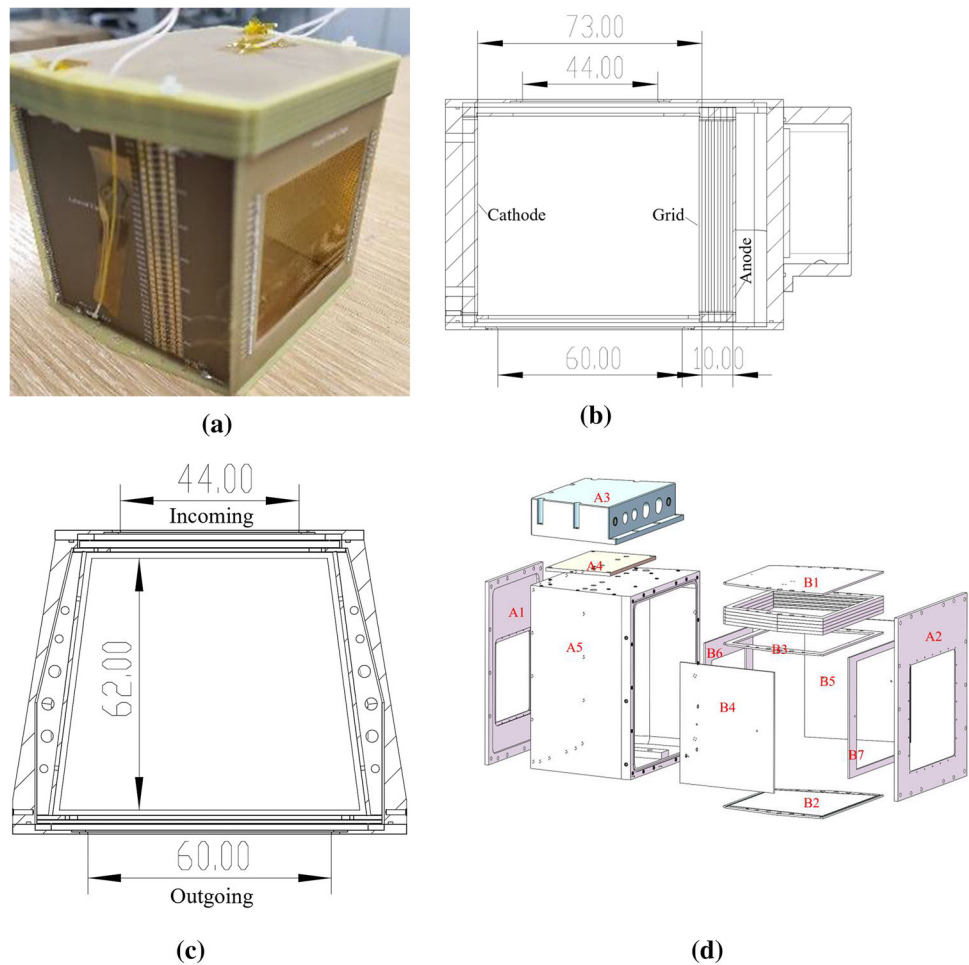


Fig. 1 Diagram and photos of a detector unit with TFG-IC as the telescope arrays: exploded diagram of the TFG-IC-based charged-particle telescope (a), side-view photo of the telescope (b) and photo of the TFG-IC array (c). The red dot (c) is the position of the reaction target in the beam experiment

Fig. 2 Photographs and schematic diagram of the TFG-IC: main internal structure (a), cross section of side view (b), cross section of top view (c) and exploded structure diagram (d). A: Aluminum box; A1-incoming window, A2-outgoing window, A3-shielding box, A4-filter board, A5-shielding case. B: TFG-IC; B1-anode, B2-cathode, B3-grid, B4-cage of side plate, B5-cage of side plate, B6-cage of incoming window, B7-cage of outgoing window



μm -thick double-sided silicon strip detector (DSSSD) manufactured by Micron Semiconductor was mounted behind TFG-IC to stop charged particles, and to enable particle identification by the $\Delta E - E$ technique. The DSSSD has an active area of $80 \times 80 \text{ mm}^2$ with 32 strips on both side; the strips on front and rear sides are mutually perpendicular. Energy measurement of high-velocity light charged particles necessitates the use of a scintillator, for which we have chosen the CsI(Tl) crystals.

We adopted a trapezoidal structure for the TFG-IC to achieve minimal detection dead area. The main internal structure of TFG-IC was made of printed circuit boards (PCB). Figure 2a–c show an exploded schematic diagram and photos of the TFG-IC-based charged-particle telescope. The ionization chamber consists of the drift region (cathode to grid), the Frisch grid, and the collection region (grid to anode). The ionization chamber grid is an electrode plate made of a PCB frame spanned with gold-plated tungsten wires of $50\text{-}\mu\text{m}$ diameter with $500\text{-}\mu\text{m}$ pitch. The cathode-grid and anode-grid distances were set to 73 mm and 10 mm, respectively. The field cage is composed of four PCBs, each with a width of 0.8 mm parallel electrode strip in steps of 1 mm etched

on both sides. The incoming and outgoing windows in the cage area were replaced by hollow PCBs spanned with gold-plated tungsten wires of $15\text{-}\mu\text{m}$ diameter to avoid energy loss of input particles. The TFG-IC was housed in separable aluminum boxes of trapezoidal geometry using $2\text{-}\mu\text{m}$ -thick mylar films as sealed windows, as shown in Fig. 2d.

Figure 3 shows the incoming and outgoing sealed windows of the ionization chamber aluminum boxes made of $2\text{-}\mu\text{m}$ -thick mylar foils with an area of $45 \text{ mm} \times 45 \text{ mm}$ and $60 \text{ mm} \times 60 \text{ mm}$, respectively. Two kinds of sealed windows with different structures were designed to study the influence of drift electric field uniformity on the detector performance. The first structure is a double-sided aluminized mylar film structure (DSA), as shown by the photo denoted by the label “L” in Fig. 3a, b. A split-strip aluminized mylar film window (SSA) was designed as the second structure. In order to provide electric field compensation, single-sided aluminized mylar was used for the SSA sealed windows which has 4-mm wide strips and 1-mm wide gaps, as shown by the photo denoted by the label “R” in Fig. 3a, b. The electric connection with the drifting field cage is completed using a spring crimp connection. Hence, the electrode centers of the sealed

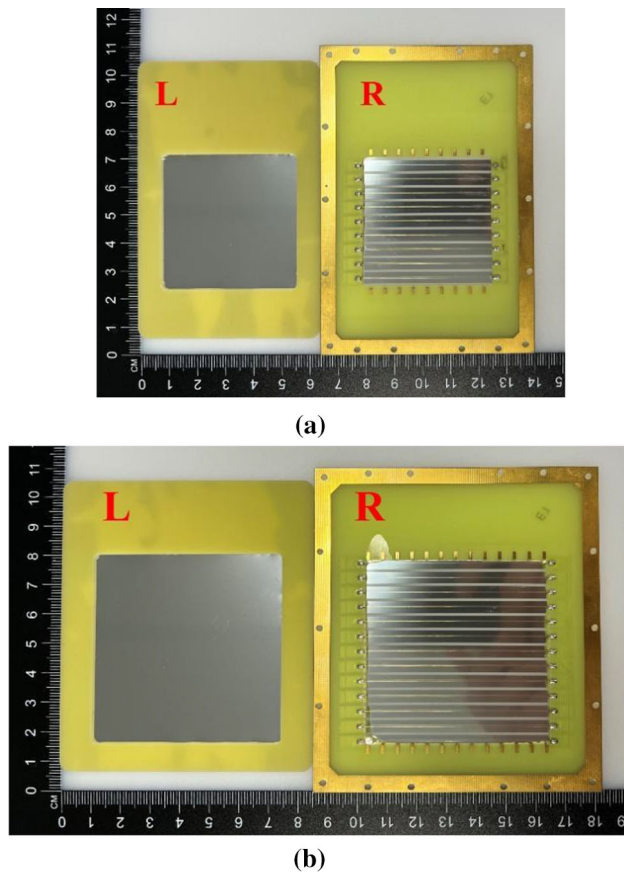


Fig. 3 Comparison of incoming sealed window (a) and outgoing sealed window (b). L: a double-sided aluminized mylar film structure window, R: a Split-strip Aluminized mylar film structure window

windows have the same voltage as the corresponding field cage electrodes.

2.2 TFG-IC operating condition

2.2.1 Working gas and voltage setting

The operation voltages of the detector were determined following the pioneering FG-IC work by Li et al. [24], which provides a relation between optimum electron transmittance and electric field ratio ($E_c: E_a$) for different wire gate; here E_c and E_a are the electric field strength between the cathode-grid and anode-grid regions, respectively. In this article, the accurate electric field ratio is 1:2.2 ($E_d: E_c$) for a Frisch grid with gold-plated tungsten wires of 50- μm diameter and a 500- μm pitch.

The detector was operated with the P10 gas (a gas mixture of 10% CH_4 and 90% argon) or CF_4 gas. When P10 was used as the working gas in the ionization chamber, the cathode voltage was set to 1000 V/bar, and the anode voltage to 300 V/bar, which correspond to a drift electric field and a collection electric field of 135 V/cm/bar and 300 V/cm/bar,

respectively [25]. Considering that CF_4 is electronegative gas, it is easier to generate electrons compared to P10 gas. Taking into account the drift rate of electrons in CF_4 , the cathode pole and anode voltages were finally set to 2000 V/bar and 600 V/bar, respectively; the electric field strength was twice that of the P10 gas. Using the Garfield++ code [26], the electron drift velocity was calculated to be about 6.4 cm/ μs at this electric field strength.

2.2.2 Electronics

In order to improve the signal-to-noise ratio, the anode voltage was supplied through an ORTEC 142PC preamplifier [27]. The anode preamplifier output signal was sent to an ORTEC 572A amplifier with a shaping time of 2 μs . The signal from the DSSSD was processed using a Mesytec MPR-16 preamplifier [28] and a Mesytec MSCF-16 main amplifier. The preamplifiers were placed inside the vacuum chamber for effective noise reduction.

The energy signal was processed and recorded using a multi-channel analyzer, ORTEC 927, when TFG-IC was measured separately. For the $\Delta E - E$ telescope test, an analog-to-digital convertor (CAEN V785 [29]) was used for the energy signals from the ionization chamber and the DSSSD. The electronics were connected as shown in Fig. 4.

2.3 Measurement of energy resolution

Using an ^{241}Am source (5.486 MeV) for P10 gas or CF_4 gas conditions, the energy resolution of TFG-IC was measured using two different types of shielding windows. Full-energy(E) and partial-energy(ΔE) deposition measurements were performed at gas pressures above 500 mbar and below 250 mbar, respectively.

2.3.1 Full-energy deposition measurement

The α source was collimated using a collimator with several small holes of about 0.5-mm diameter, placed at the center of the cathode. The electric field was kept constant during the measurement, and the range of alpha particles was controlled by changing the gas pressure. The energy resolution of the ionization chamber was recorded in relation to the working gas pressure.

2.3.2 $\Delta E - E$ telescope measurement with TFG-IC and a DSSSD detector

The α source was placed at the target position, as indicated by the red dot in Fig. 1c. α particles passed through the ionization chamber, and were stopped by the silicon detector, where the remaining energies were deposited. The energy depositions in TFG-IC and the DSSSD were measured using the P10 gas

Fig. 4 Block diagram of the electronics used in the laboratory

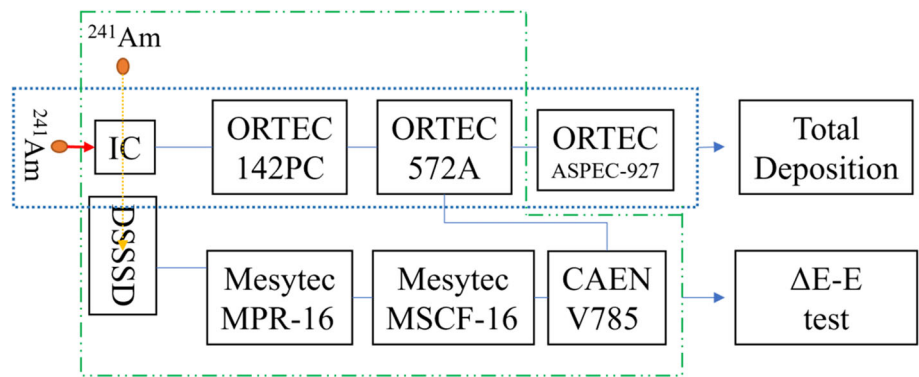
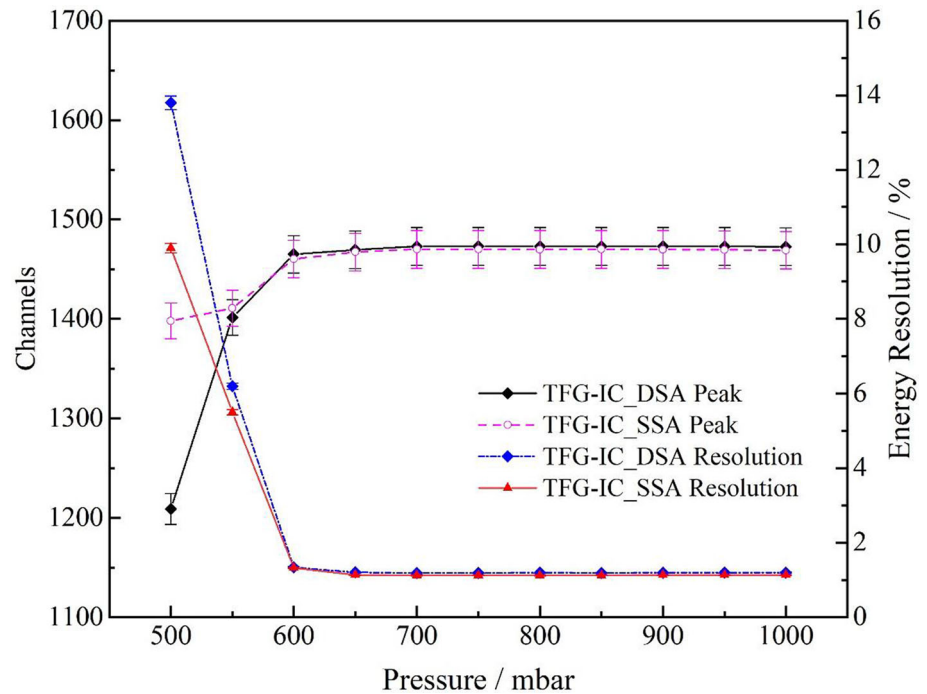


Fig. 5 The energy resolution and pulse height evolution at various working gas pressures



at 200 mbar with the DSA sealed windows. For the measurements with the SSA sealed windows, the energy depositions were measured in detail under four different pressure conditions for the P10 working gas: 100 mbar, 150 mbar, 200 mbar and 250 mbar. Since CF₄ is denser than P10, the particle energy loss is greater than that in P10 gas under the same pressure. Measurements were also performed at 100 mbar, 150 mbar and 200 mbar gas pressures for CF₄.

3 Results and discussion

3.1 Comparison of TFG-IC with different shielding structure

3.1.1 Comparison of total energy deposition for α source

According to the calculation using the Stopping and Range of Ions in Matter (SRIM) code [30], the projected range of

a 5.5 MeV alpha particle is around 5 cm in the P10 gas at 1013 mbar. The minimum pressure of the P10 gas should be above 600 mbar to stop alpha particles with kinetic energy of 5.486 MeV from ²⁴¹Am. The energy resolution and peak position as functions of the working gas pressure were measured with an ²⁴¹Am source for the types of sealed windows, and the results are shown in Fig. 5. The energy resolution remains stable beyond the minimum pressure. No significant difference was observed between the results with two different sealed windows. The reason may be that the collimation hole set at the cathode is too small, which leads to a small oblique incidence of α particles in the sensitive volume, and the ionized electrons hardly pass through the area with large electric field distortion.

Figure 6 presents the energy spectra obtained at 700 mbar of the P10 gas with an ²⁴¹Am source for the different sealed windows. The red lines represent the best-fitted Gaussian peak taking into account the known alpha peak energies and

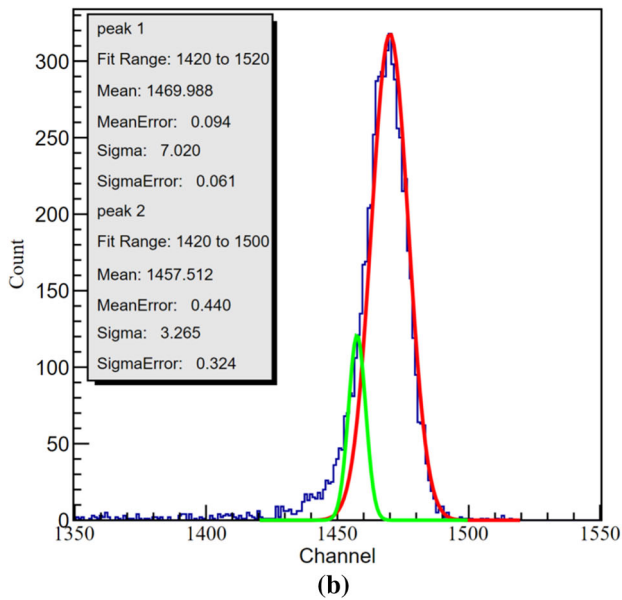
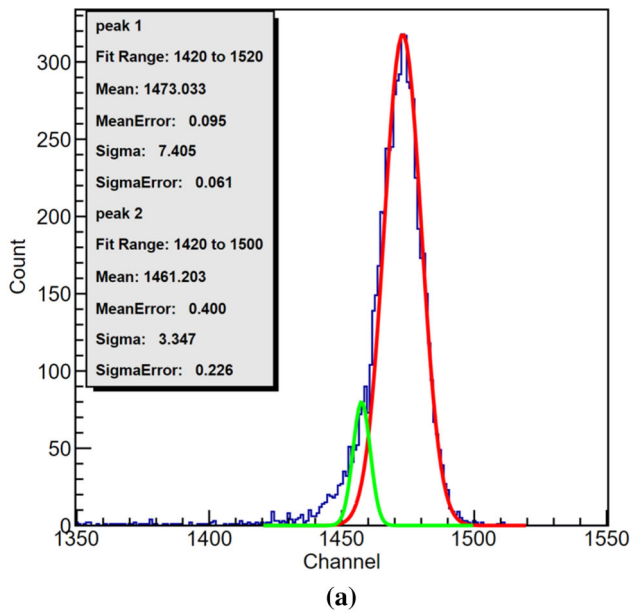


Fig. 6 Energy spectra obtained with an ²⁴¹Am source at 700 mbar for two different sealed windows of the ionization chamber: **a** DSA sealed windows, and **b** SSA sealed windows. The red lines (on top of the data) represent the total adjustment to the data taking into account the known alpha peak energies (5.48556 MeV) and branching ratios (84.8%), while the green lines refer to the alpha peak energies (5.44428 MeV) and branching ratios (13.1%)

branching ratios The energy resolution was calculated using the full width at half maximum (FWHM) and peak position of the main alpha (5.48556 MeV) decay branch with a branching ratio of 84.8% [24]. Throughout all of the measurements, we used identical methods to determine the FWHM and the peak position. The energy resolution of TFG-IC was 1.1% (FWHM), as presented in Fig. 6.

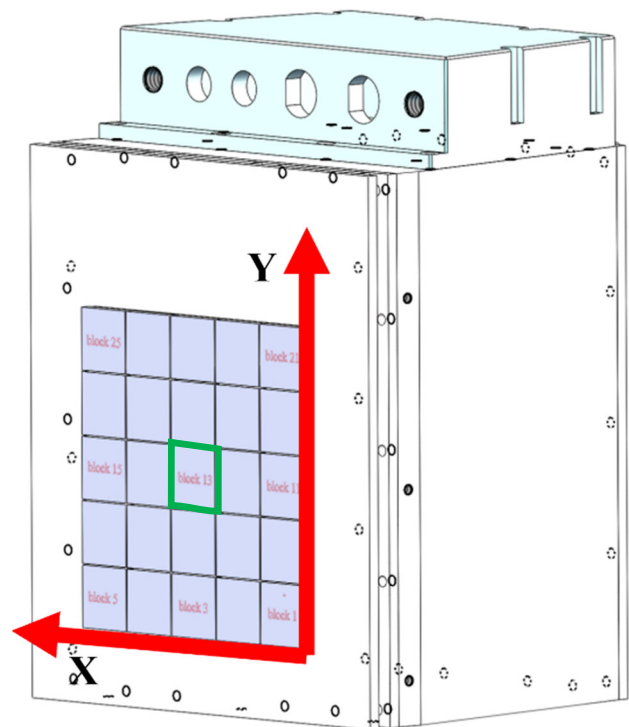


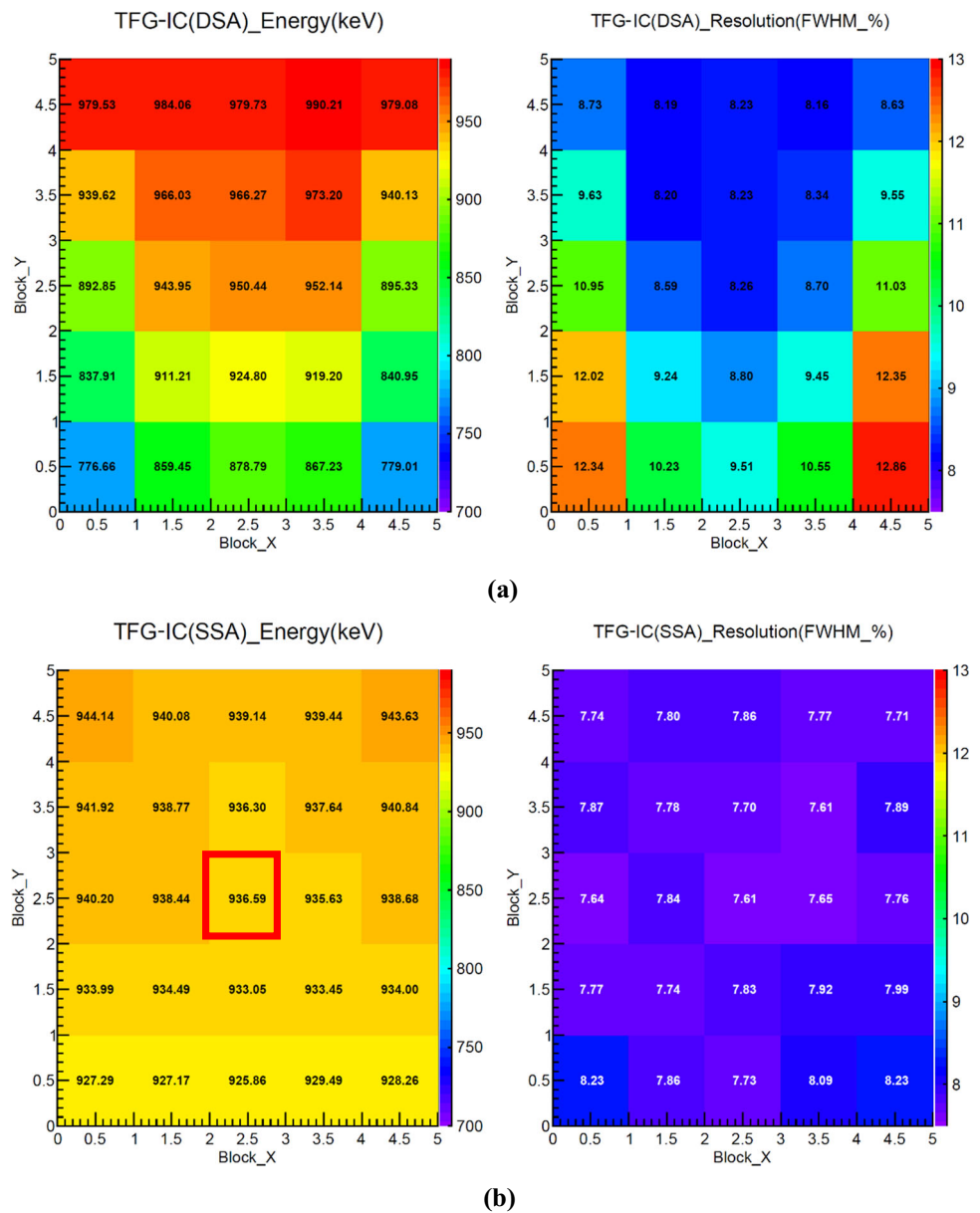
Fig. 7 Diagram of the block ID definition. The green frame refers to block 13

3.1.2 Comparison of $\Delta E-E$ for α source

The $\Delta E - E$ performance of the TFG-IC+DSSSD telescope was tested with an ²⁴¹Am source to verify the effect of different sealed windows. Besides the energy information, the DSSSD also provided two-dimensional position information of the α particles. The exit window of TFG-IC was divided into 25 blocks to identify and separate α particles of different incident tracks. The block ID definition is shown in Fig. 7. The energy losses of α particles on different paths in the ionization chamber were obtained using the position information of the DSSSD.

Figure 8 shows the main peak and resolution of energy spectra of α particles at 200 mbar pressure of the P10 gas measured in different blocks of the ionization chamber with two different sealed windows. Fluctuations are indicated by different colours as shown on the right of each histogram. The average fluctuation of the energy loss in the ionization chamber with SSA sealed windows is about 20 keV, which is excellent compared with the DSA sealed windows. The energy resolution with the SSA sealed windows also has a smaller fluctuation than that with the DSA sealed windows; the former is only about 1% whereas the latter is about 4%. The results show that the ionization chamber with the SSA sealed windows is significantly better than that of the DSA ones.

Fig. 8 Energy spectra of alpha particles measured in different areas of the longitudinal section of two different structures of ionization chambers at 200 mbar pressure with DSA structure sealed windows (a) and with SSA structure sealed window (b). The red frame (b) refers to block 13 in Fig. 7



3.2 Simulation of electric field uniformity

The results in Fig. 8 show the better performance of the ionization chamber with SSA sealed windows. To better understand the response and performance of the detector, we performed simulation to estimate the two-dimensional electric field in the drift region for the two different sealed windows using COMSOL [31], as shown in Fig. 9. It is found from the Fig. 9a that the electric field in the drift region with the DSA sealed windows has a relatively large distortion near the incoming and outgoing windows. The edge effect caused by the distortion of the electric field will cause the performance of the detector to deteriorate due to the loss of some electrons in the sensitive volume of the ionization chamber. The simulation result with the SSA sealed windows is shown in Fig. 9b, where the electric field distortion at the edge is

found to be significantly smaller than the electric field compensation. These simulation results explain the difference in the performance as shown in Fig. 8 due to different field-cage electric field.

3.3 $\Delta E - E$ measurement with the SSA structure using three-component α source

A three-component α source (^{239}Pu , ^{241}Am , ^{244}Cm) was used to test and calibrate the detector. Measurements were performed for the TFG-IC+DSSSD telescope system with the SSA sealed windows at 250 mbar pressure of the P10 gas. Using the measured energy ΔE deposited in TFG-IC and the residual energy E deposited in the DSSSD, we obtained the $\Delta E - E$ correlation; typical spectra for the block 13 defined

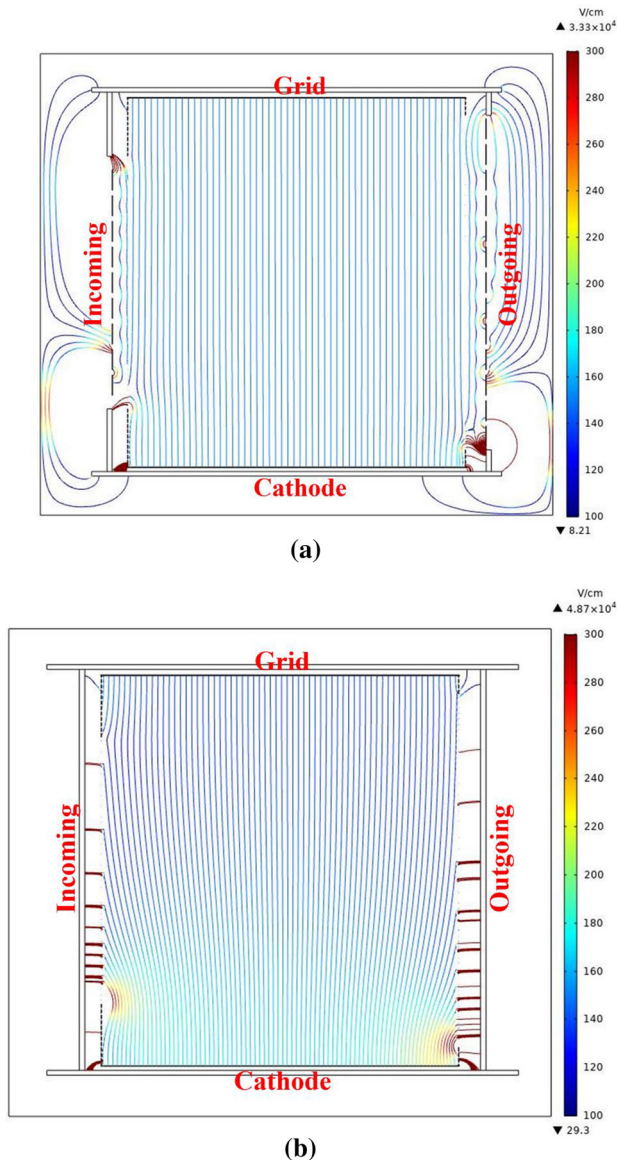


Fig. 9 Field cage electric field distribution of DSA structure sealed window (a) and SSA structure sealed window (b). The Cross section is the side view of detector which is shown in the Fig. 2b

in Fig. 7 are shown in Fig. 10. Overall, our telescope system can resolve well alpha particles with different energies.

3.4 Energy-loss measurement with the SSA sealed windows at various gas pressures

Since the energy loss of a particle in a gas detector depends on the gas pressure and gas species of the detector, one can easily manipulate the energy loss in the detector, which is an important advantage of the gas detector. To evaluate the performance of TFG-IC with the SSA sealed windows, the energy loss ΔE and energy resolution were measured at four and three different pressures for the P10 and CF₄ gases,

respectively. Figure 11 shows the relationship between the measured energy and the energy resolution of the ionization chamber at different gas pressures using an α source. The first four points in Fig. 11 are the results for the P10 gas, while the last two points for the CF₄ gas; the third point for the CF₄ gas is not plotted since all α particles are stopped in TFG-IC at 200 mbar pressure.

It is difficult to measure energy loss and energy resolution over a wide range using a monoenergetic α source. Using the results in Fig. 11, we fitted the data by the least-squares method (χ^2) to extrapolate the detector operational domain to the low-energy and high-energy regions. The fitted curve will be applied in simulations or future experiments.

3.5 Simulation of particle identification (PID) using extrapolating curves

In order to simulate the operation of the ionization chamber in a beam experiment, we set up a model according to the experimental setup shown in Fig. 12 in Geant4 [32], taking into account the 2- μ m-thick mylar shielding window, dead zone, sensitive volume and silicon detector. In the simulation, the expansion of the dead zone and the bulge of the sealed window due to the pressure difference of the gas detector were ignored. Simulations were performed for p , d , t , ^3He , ^4He , ^6He , ^6Li , ^7Li , ^9Be , ^{11}B and ^{12}C assuming all incident particles enter the detector at angles perpendicular to the shield window. The P10 gas at 200 mbar and CF₄ at 150 mbar are used as the working gases of the ionization chamber. The extrapolation curves obtained in Fig. 11 were implemented in the simulation as an intrinsic correlation function of the ionization chamber.

Using the simulation data, a two-dimensional $\Delta E - E$ scatter plot of TFG-IC+DSSSD was constructed for each telescope and determined for all isotopes, as shown in Fig. 13. When the P10 gas at 200 mbar is used as the working gas, p , d and t particles cannot be separated in the low-energy region, but good PID can still be achieved for ^3He , ^4He and ^6He . On the other hand, p , d and t particles can be separated in the low-energy region using the CF₄ gas at 150 mbar pressure as the working gas, as shown in Fig. 13b. Therefore, when using an ionization chamber, it is necessary to select the appropriate working gas, taking into consideration the experimental requirements and by combining the simulation results.

4 Conclusions

We have designed and developed a new TFG-IC as the first layer of charged-particle telescopes. Performing measurements with an ^{241}Am source and simulations, we compared the energy resolution and energy deposition for two different

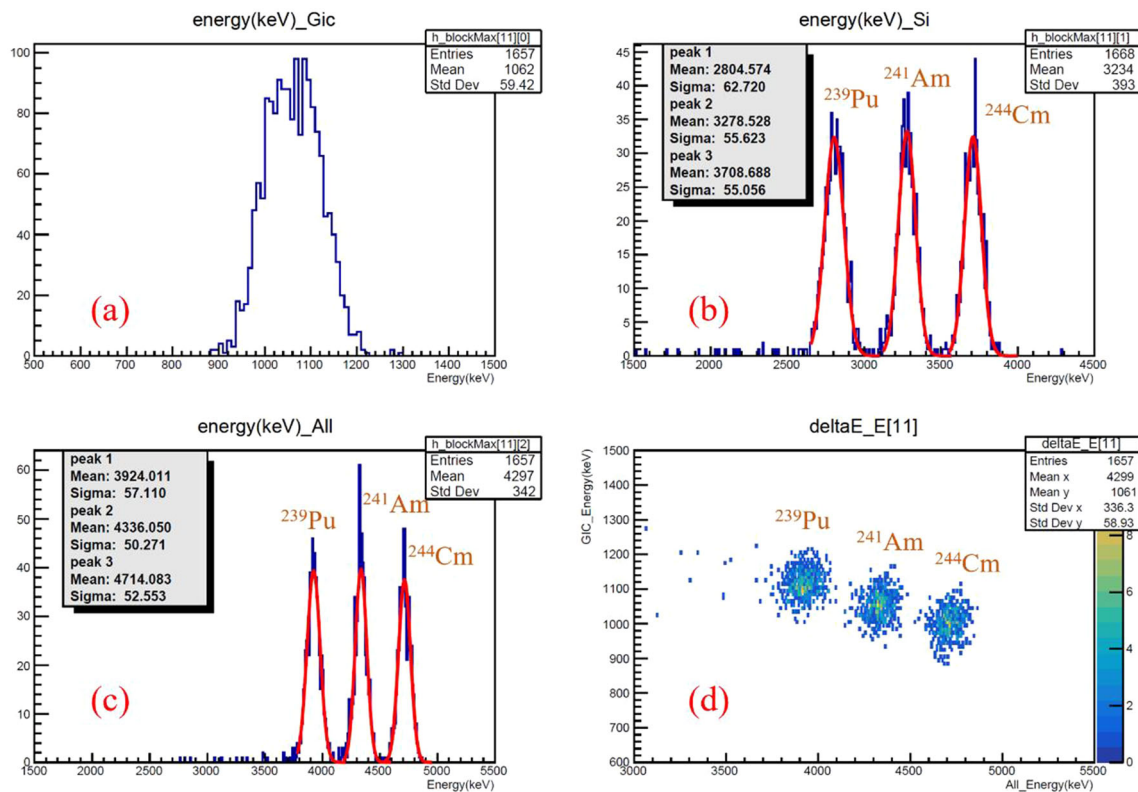


Fig. 10 Results of the measurement with a three-component alpha source for the telescope system with the SSA sealed windows: **a** the ΔE (energy deposit) spectrum of TFG-IC, **b** E deposited in the DSSSD, **c**

total energy $\Delta E + E$ spectrum, and **d** two-dimensional scatter plot showing correlation between ΔE and total energy

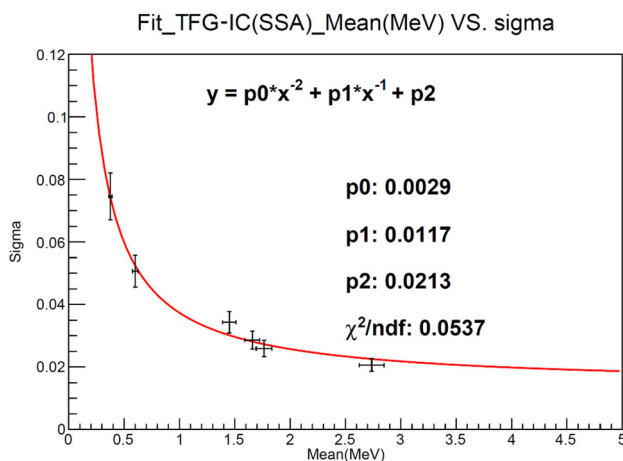


Fig. 11 Fitted extrapolated ionization chamber at different gas pressures measured energy and energy resolved. The first four points and the last two points are obtained using the P10 and CF₄ gases, respectively

sealed windows. The result shows that TFG-IC with the SSA sealed windows offers more stable performance. We tested the TFG-IC+DSSSD telescope with the SSA sealed windows in detail by varying the gas pressure of the P10 or CF₄ gas using an α source. An extrapolation curve was obtained

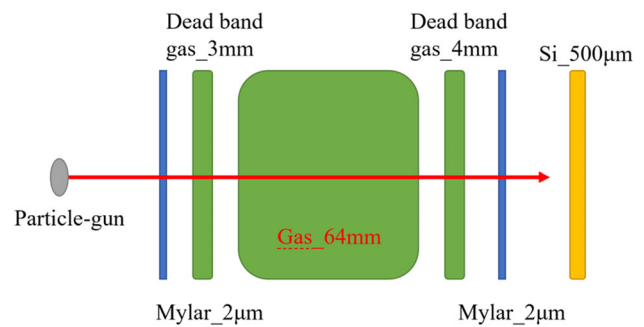


Fig. 12 Simulation geometry setup model in Geant4

by fitting the correlated data of TFG-IC for different energy loss and energy resolution using the least-squares method. The extrapolation curve is used in simulations with Geant4 to evaluate the PID capability of the $\Delta E - E$ telescope system with TFG-IC. It can be seen from the simulation results that the $\Delta E - E$ telescope system consisting of an ionization chamber can easily distinguish between protons and alpha particles. Using denser gas, such as CF₄, the $\Delta E - E$ telescope system may also be able to separate p , d and t .

In summary, we present in this article the Advanced Mass Estimate (AME), a new approach based upon the telescope

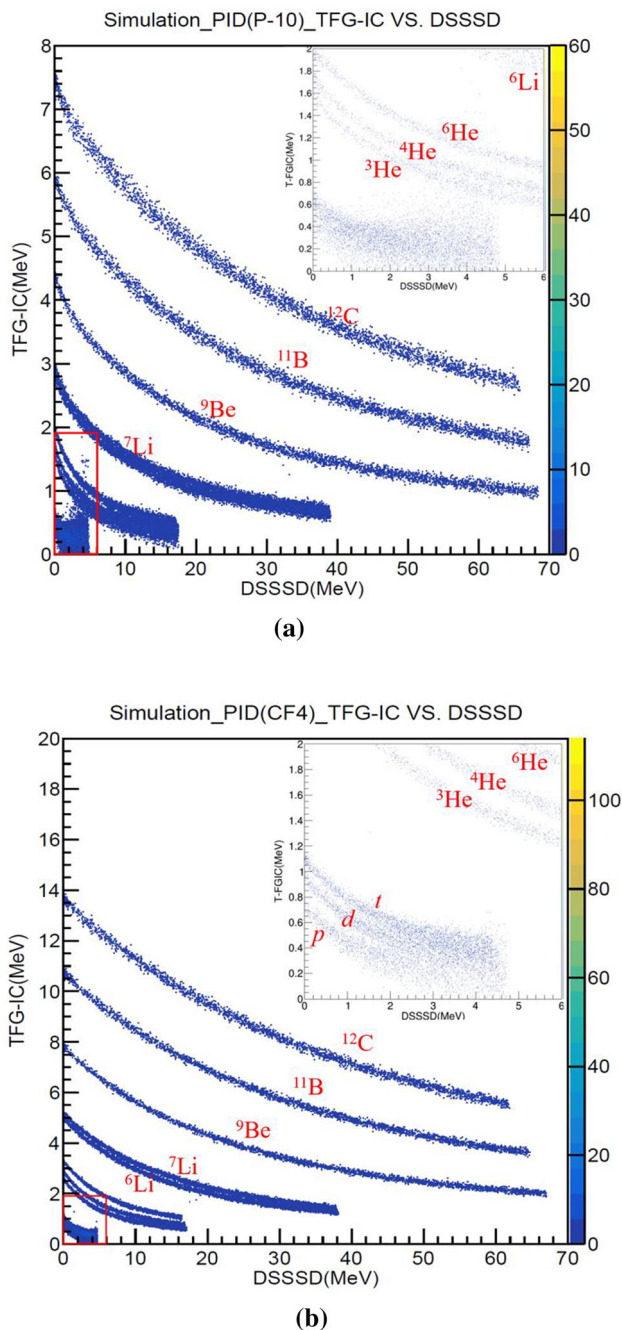


Fig. 13 ΔE - E correlation in the TFG-IC + DSSSD telescope for simulated data: Working gas P10 (a) and Working gas CF₄ (b)

technique using TFG-IC. This method will extend the isotopic identification to heavier nuclear-reaction products.

Acknowledgements This work is financially supported by the National Key R&D Program of China (Grant no. 2018YFE0205200), the Strategic Priority Research Program of Chinese Academy of Sciences (Grant no. XDB34000000), the Research Program of National Major Research Instruments (Grant no. 11927901), the National Science Foundation of China (Grant no. 11875301, 11875302, U1867214, U1832105, U1832167), and the CAS “Light of West China” Program. This work

is also supported by the Function Development Project of Chinese Academy of Sciences under Grant no. 2022G101.

Data Availability Statement This manuscript has no associated data or the data will be deposited. [Authors’ comment: as for the data availability, the only data relevant to the publication is present in form of published graphs or tables. All the datasets and figures in the paper can be available from the corresponding authors upon request].

Open Access This article is licensed under a Creative Commons Attribution 4.0 International License, which permits use, sharing, adaptation, distribution and reproduction in any medium or format, as long as you give appropriate credit to the original author(s) and the source, provide a link to the Creative Commons licence, and indicate if changes were made. The images or other third party material in this article are included in the article’s Creative Commons licence, unless indicated otherwise in a credit line to the material. If material is not included in the article’s Creative Commons licence and your intended use is not permitted by statutory regulation or exceeds the permitted use, you will need to obtain permission directly from the copyright holder. To view a copy of this licence, visit <http://creativecommons.org/licenses/by/4.0/>.

Funded by SCOAP³. SCOAP³ supports the goals of the International Year of Basic Sciences for Sustainable Development.

References

1. M. Di Giacomo, R. Ferdinand, B. Jacquot et al., Proton beam commissioning of the SPIRAL2 Single Bunch Selector. *J. Instrum.* **15**(12), T12011 (2020). <https://doi.org/10.1088/1748-0221/15/12/T12011>
2. T. Marchi, G. Prete, F. Gramegna et al., The SPES facility at Legnaro National Laboratories. *J. Phys.: Conf. Ser.* **1643**(1), 012036 (2020). <https://doi.org/10.1088/1742-6596/1643/1/012036>
3. G. Rosner, Future facility: FAIR at GSI. *Nucl. Phys. B (Proc. Suppl.)* **167**, 77–81 (2006). <https://doi.org/10.1016/j.nuclphysbps.2006.12.089>
4. A. Gade, B.M. Sherrill, NSCL and FRIB at Michigan State University: nuclear science at the limits of stability. *Phys. Scr.* **91**(5), 053003 (2016). <https://doi.org/10.1088/0031-8949/91/5/053003>
5. T. Suda, Present status of the RIKEN Radioactive Ion Beam Factory, RIBF. *J. Phys.: Conf. Ser.* **267**(1), 012008 (2011). <https://doi.org/10.1088/1742-6596/267/1/012008>
6. G. Raciti, E. Rapisarda, M. De Napoli et al., Intermediate energies tagged RIBs. *Nucl. Inst. Methods Phys. Res. B* **266**, 19–20 (2008). <https://doi.org/10.1016/j.nimb.2008.05.153>
7. Z. Sun, W.-L. Zhan, Z.-Y. Guo et al., RIBLL, the radioactive ion beam line in Lanzhou. *Nucl. Inst. Methods Phys. Res. A* **503**(3), 496–503 (2003). [https://doi.org/10.1016/S0168-9002\(03\)01005-2](https://doi.org/10.1016/S0168-9002(03)01005-2)
8. E. Pollacco, D. Beaumel, P. Roussel-Chomaz et al., MUST2: a new generation array for direct reaction studies. *Eur. Phys. J. A* **25**(1), 287–288 (2005). <https://doi.org/10.1140/epjad/i2005-06-162-5>
9. J. Pouthas, B. Borderie, R. Dayras et al., INDRA, a 4 π charged product detection array at GANIL. *Nucl. Inst. Methods Phys. Res. A* **357**, 418 (1995). [https://doi.org/10.1016/0168-9002\(94\)01543-0](https://doi.org/10.1016/0168-9002(94)01543-0)
10. O. Lopez, M. Pârlog, B. Borderie et al., Improving isotopic identification with INDRA Silicon-CSi(Tl) telescopes. *Nucl. Inst. Methods Phys. Res. A* **884**, 140–149 (2018). <https://doi.org/10.1016/j.nima.2017.12.041>
11. B. Davin, R.T. de Souza, R. Yanez et al., LASSA: a large area silicon strip array for isotopic identification of charged particles. *Nucl. Inst. Methods Phys. Res. A* **473**(3), 302–318 (2001). [https://doi.org/10.1016/S0168-9002\(01\)00295-9](https://doi.org/10.1016/S0168-9002(01)00295-9)

12. S. Wuenschel, K. Hagel, R. Wada et al., NIMROD-ISiS, a versatile tool for studying the isotopic degree of freedom in heavy ion collisions. *Nucl. Inst. Methods Phys. Res. A* **604**(3), 578–583 (2009). <https://doi.org/10.1016/j.nima.2009.03.187>
13. G. Verde, L. Acosta, T. Minniti et al., The Farcos project: femtoscope array for correlations and femtoscopy. *J. Phys.: Conf. Ser.* **420**, 012158 (2013). <https://doi.org/10.1088/1742-6596/420/1/012158>
14. L. Acosta, R. Andolina, L. Auditore et al., Campaign of measurements to probe the good performance of the new array FARCOS for spectroscopy and correlations. *J. Phys.: Conf. Ser.* **730**(1), 012001 (2016). <https://doi.org/10.1088/1742-6596/730/1/012001>
15. R. Bougault, G. Poggi, S. Barlini et al., The FAZIA project in Europe: R&D phase. *Eur. Phys. J. A. Hadrons Nucl.* **50**(2), 1–20 (2014). <https://doi.org/10.1140/epja/i2014-14047-4>
16. F. Guan, Y. Wang, X. Diao et al., Track recognition of ΔE_E telescopes with silicon strip detectors. *Nucl. Inst. Methods Phys. Res. A* **1029**, 166461 (2022). <https://doi.org/10.1016/j.nima.2022.166461>
17. F. Guan, X. Diao, Y. Wang et al., A compact spectrometer for heavy ion experiments in the Fermi energy regime. *Nucl. Inst. Methods Phys. Res. A* **1011**, 165592 (2021). <https://doi.org/10.1016/J.NIMA.2021.165592>
18. H. Wang, G. Fan, L. Liu et al., Development and prospect of Shanghai laser Compton scattering gamma source. *Nucl. Phys. Rev.* **37**(01), 53–63 (2020). <https://doi.org/10.11804/NuclPhysRev.37.2019043>
19. Y. Zhao, R. Fan, Q. Zhang et al., Particle identification technique using grid ionization chamber at China Spallation Neutron Source. *J. Instrum.* **12**(11), P11001 (2017). <https://doi.org/10.1088/1748-0221/12/11/P11001>
20. T. Wang, H. Han, Q. Meng et al., Measurements of charge distributions of the fragments in the low energy fission reaction. *Nucl. Inst. Methods Phys. Res. A* **697**, 7–12 (2013). <https://doi.org/10.1016/j.nima.2012.08.109>
21. I. Harayama, K. Nagashima, Y. Hirose et al., Development of $\Delta E - E$ telescope ERDA with 40 MeV $^{35}\text{Cl}^{7+}$ beam at MALT in the University of Tokyo optimized for analysis of metal oxynitride thin films. *Nucl. Instrum. Methods Phys. Res. B* **384**, 61–67 (2016). <https://doi.org/10.1016/j.nimb.2016.07.019>
22. M. Romoli, L. Morales Gallegos, M. Aliotta et al., Development of a two-stage detection array for low-energy light charged particles in nuclear astrophysics applications. *Eur. Phys. J. A* **54**(8), 1–8 (2018). <https://doi.org/10.1140/epja/i2018-12575-5>
23. N. Ma, C. Lin, J. Wang et al., A multilayer $\Delta E - E_R$ telescope for breakup reactions at energies around the Coulomb barrier. *Chin. Phys. C* **40**(11), 132–136 (2016). <https://doi.org/10.1088/1674-1137/40/11/116004>
24. M. Li, Y. Yang, P. Ma et al., Exploration of grid scheme for Frisch-grid ionization chamber. *Eur. Phys. J. C* **81**(12), 1–9 (2021). <https://doi.org/10.1140/EPJC/S10052-021-09879-Y>
25. M. Li, Z. He, C. Xiao et al., Grid ionization chamber based on stainless steel woven wire mesh. *J. Instrum.* **17**(08), P08038 (2022). <https://doi.org/10.1088/1748-0221/17/08/P08038>
26. S.F. Biagi, Magboltz, program to compute gas transport parameters, Version 11 (CERN, 2021)
27. AMETEK ORTEC. <https://www.ortec-online.com.cn/>
28. MESYTEC, Detector Readout System. <https://www.mesytec.com/>
29. CAEN-Tools for Discovery. <https://www.caen.it/>
30. SRIM-The Stopping and Range of Ions in Matter. <http://www.srim.org/>
31. COMSOL, Multiphysics (2021). <https://cn.comsol.com/>
32. Geant4—a simulation toolkit. <https://geant4.web.cern.ch/>